VIP Catalysis Mechanisms Very Important Paper

International Edition: DOI: 10.1002/anie.201709652
German Edition: DOI: 10.1002/ange.201709652

The Common Intermediates of Oxygen Evolution and Dissolution Reactions during Water Electrolysis on Iridium

Olga Kasian, Jan-Philipp Grote, Simon Geiger, Serhiy Cherevko, and Karl J. J. Mayrhofer*

Abstract: *Understanding the pathways of catalyst degradation during the oxygen evolution reaction is a cornerstone in the development of efficient and stable electrolyzers, since even for the most promising Ir based anodes the harsh reaction conditions are detrimental. The dissolution mechanism is complex and the correlation to the oxygen evolution reaction itself is still poorly understood. Here, by coupling a scanning flow cell with inductively coupled plasma and online electrochemical mass spectrometers, we monitor the oxygen evolution and degradation products of Ir and Ir oxides in situ. It is shown that at high anodic potentials several dissolution routes become possible, including formation of gaseous IrO_3. On the basis of experimental data, possible pathways are proposed for the oxygen-evolution-triggered dissolution of Ir and the role of common intermediates for these reactions is discussed.*

The oxygen evolution reaction (OER) plays a crucial role in the development of efficient electrolyzers for energy conversion and storage.[1] The sluggish kinetics[2] of this reaction and instability of most of the catalyzing materials[3] remain serious challenges for the optimization of the existing technology towards cost-competitive commercialization.[4] Currently, proton-exchange membrane water electrolyzers rely on iridium-based materials, providing a compromising combination of relatively high catalytic activity and durability.[5] However, even Ir-based anodes slowly undergo dissolution under operation conditions of the OER.[6] Considering the low abundance and high price of Ir, understanding the kinetics and mechanism of its electrochemical dissolution is of high importance for a knowledge-based improvement of performance.[7] Kinetic parameters of the Ir dissolution reaction can be determined by electrochemical methods[8] or more directly by utilizing sensitive analytical methods such as, for example, inductively coupled plasma mass spectrometry (ICP-MS).[9] Mechanistic studies of both OER and dissolution at the solid–liquid interface are more challenging, as they typically require detection of reaction intermediates with short lifetimes. Since experimental data on intermediates have been inaccessible so far, possible mechanisms are the subject of intensive debate in the literature.[7,10] Most of the proposed pathways of OER on metallic Ir and its oxides were based on measurements on hydrous or anodically formed oxide films. A recent OER mechanism in acidic media suggested in a number of studies[7,11] includes the participation of Ir^{III} species, which are considered crucial for high activity. During anodic polarization of hydrous oxide in acid[12] Ir^{III}–Ir^{V} oxidation state switching was also shown to occur. The formation of Ir^{V} and Ir^{III} intermediates during OER was confirmed experimentally by application of XAS-[12] and XPS-based techniques.[13] Additionally, the OER on IrO_2 nanoparticles was suggested to proceed via Ir^{IV}–Ir^{V} transformation.[13a] The role of the abovementioned intermediates for the stability of Ir, however, was not discussed in this work. In our previous study using the data on the dissolution rates of metallic Ir and hydrous Ir oxide, stability was suggested to correlate to the activity and thus the Ir^{III}–Ir^{V} transformation was proposed.[9,14] Interestingly, another possible route for OER-triggered Ir degradation was suggested to occur via formation of volatile iridium species in the Ir^{VI} oxidation state, assuming similarities between Ir and Ru.[15] Specifically, Kötz et al. proposed such a route based on the data of Wohlfahrt-Mehrens and Heitbaum, who showed with the aid of differential or online electrochemical mass spectrometry (DEMS/OLEMS) that Ru dissolves via the formation of volatile RuO_4 during OER.[16] DEMS- and OLEMS-based techniques were also utilized to shed some light on the mechanism of OER on Pt,[17] Ru,[18] IrO_2,[19] and non-noble perovskites;[2] however, dissolution was out of the scope of these studies and formation of volatile Ir oxides during the OER has not yet been confirmed experimentally.

Here we utilized a scanning flow cell (SFC) coupled with OLEMS to further resolve the degradation pathway of metallic Ir and its oxides (thermally formed or reactively sputtered) and the correlation to the OER mechanism. The high sensitivity of our setup allows us to detect minor amounts of volatile products. Additionally, the activity and stability of these electrodes are investigated in parallel by a SFC connected to ICP-MS (see arrangement of setups in Figure S1).

[*] Dr. O. Kasian, Dr. J.-P. Grote, Dr. S. Geiger, Dr. S. Cherevko, Prof. K. J. J. Mayrhofer
Max-Planck-Institut für Eisenforschung GmbH
Max-Planck-Strasse 1, 40237 Düsseldorf (Germany)
E-mail: o.kasian@mpie.de
Dr. S. Cherevko, Prof. K. J. J. Mayrhofer
Helmholtz-Institute Erlangen-Nürnberg for Renewable Energy
IEK-11, Forschungszentrum Jülich GmbH
Egerlandstrasse 3, 91058 Erlangen (Germany)
Prof. K. J. J. Mayrhofer
Department of Chemical and Biological Engineering
Friedrich-Alexander-Universität Erlangen-Nürnberg
Egerlandstrasse 3, 91058 Erlangen (Germany)
Supporting information and the ORCID identification number(s) for the author(s) of this article can be found under: https://doi.org/10.1002/anie.201709652.

Details regarding the electrode preparation and characterization are presented and discussed in the Supporting Information. In short, the composition of the as-prepared metallic Ir film and its oxides was confirmed using X-ray photoelectron spectroscopy (Figures S2–S4). Both reactively sputtered and thermally formed oxides consist of IrO_2 only (Figures S3 and S4), while the as-prepared Ir film shows only a metallic phase (Figure S2). Considering that the evolution of oxygen always results in oxidation of the electrode, the term "metallic Ir electrode" refers to an electrochemically formed oxide formed during short-term polarization.

The summarized data on the stability of the thermally formed Ir oxide (thermal oxide) is exemplarily presented in Figure 1. The electrode is polarized at 5, 10, 15, and

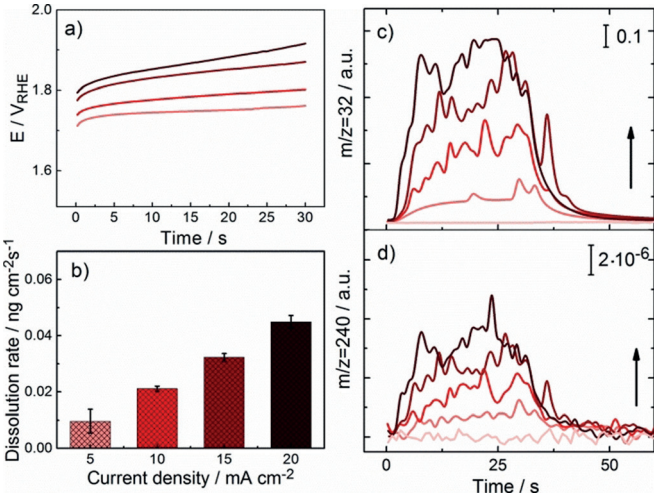

Figure 1. a) Measured potential during 30 s of anodic polarization of Ir thermal oxide in 0.1 M $HClO_4$ at 5, 10, 15, and 20 mA cm^{-2} at room temperature. b) Average rate of iridium dissolution as measured online with ICP-MS. Mass spectra of c) O_2 (m/z 32) and d) IrO_3 (m/z 240) acquired online with OLEMS. The color gradient indicates the increase of applied current density from 5 mA cm^{-2} to 20 mA cm^{-2}. The baselines in (c) and (d) show the O_2 (m/z 32) and IrO_3 (m/z 240) signals measured at the open circuit potential.

20 mA cm^{-2} during 30 s and the corresponding values of potential (a) and the average dissolution rate of Ir (b) are measured online. Simultaneously, the volatile species with mass-to-charge ratios (m/z) of 32 (c) and 240 (d) formed during the OER are measured in situ (see Figures 1 and S5). In line with dissolution, the formation of O_2 and IrO_3 becomes more pronounced at higher current densities (Figure 1 c,d). Metallic Ir and reactively sputtered oxide show the same trend and increase in both dissolution and IrO_3 formation with increasing current density (see Figures S6 and S7, respectively). For thermal oxide, formation of IrO_3 is observed already at 5 mA cm^{-2}, while the evolution of this volatile intermediate on metallic Ir and reactively sputtered IrO_2 is negligible or even absent at low current densities.

Considering the OER as the main anodic reaction on iridium oxides, polarization of different electrodes at the same current density leads to an equal amount of evolved O_2. However, at the identical current density conditions both the stability and the formation of IrO_3 strongly depend on the nature of the Ir anode, as well as on the different values of potential imposed by these electrodes.

For a semiquantitative estimation of the interplay between the activity and the formation of IrO_3, the integrated signal of m/z 240 and the value of potential at the end of polarization were plotted versus applied current density (Figure 2 b,c). Both dissolution of Ir and formation of volatile

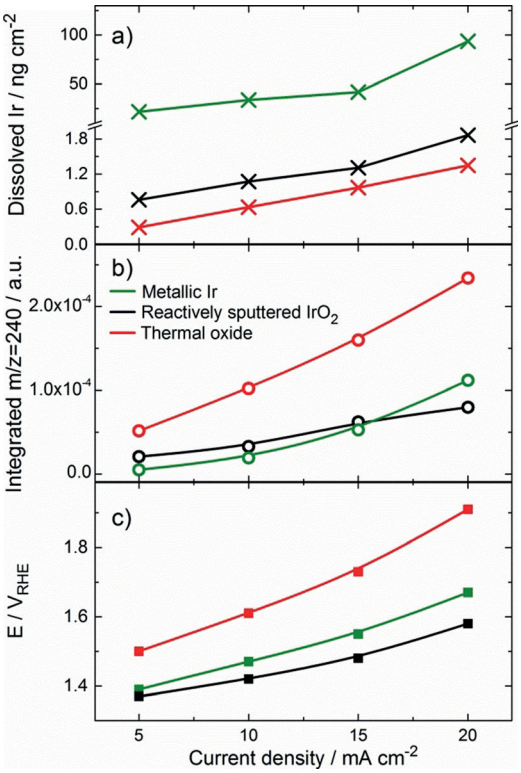

Figure 2. Dependence of a) the amount of dissolved Ir, b) the formation of IrO_3 and potential at the end of polarization on the current density obtained for metallic Ir (green), reactively sputtered IrO_2 (black) and thermal IrO_2 (red).

IrO_3 clearly depend on the value of applied current density and the nature of the electrode. At high current densities, dissolution of metallic Ir is about two orders of magnitude higher than for thermal or reactively sputtered oxides (Figure 2 a). Considering the lower value of potential on metallic Ir (Figure 2 c), the dominating dissolution mechanism on this electrode includes formation of intermediates in an oxidation state lower than Ir^{VI}, for example, Ir^{III} or Ir^{V}. During anodic polarization metallic Ir^0 can undergo direct dissolution forming soluble Ir^{3+} and further transform to IrO_2 [see Scheme 1, Eqs. (S1) and (S2)]. Additional dissolution of metallic Ir beneath the non-uniform oxide film is also possible. One should consider, however, that direct dissolution Ir^0–Ir^{3+} becomes less favorable with increasing oxide coverage on the metal surface and obviously does not occur on thermal or reactively sputtered oxides. Consequently, reactively sputtered IrO_2 with similar electrocatalytic activity to metallic Ir is significantly less prone to dissolution. the superior electrocatalytic behavior of reactively sputtered IrO_2

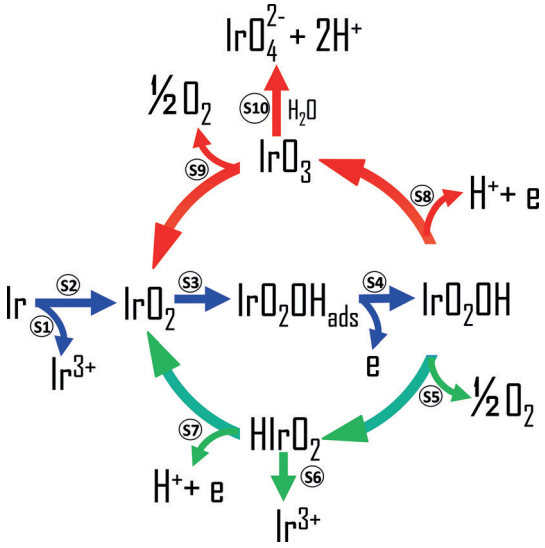

Scheme 1. Simplified scheme showing possible pathways of Ir dissolution during the OER. Green arrows indicate the mechanism that is preferable for electrocatalytically active Ir-based materials where OER occurs at lower potentials. Red arrows present the dissolution route dominating at higher anodic potentials. Blue arrows show intermediate steps that take place regardless of the electrode material and potential. Corresponding equations can be found in the Supporting information.

was first presented by Beni et al.[5a] and will be further discussed in future work.

The low dissolution of thermal IrO_2 with rutile structure (Figure S4) can be explained by its thermodynamic stability and was discussed elsewhere.[6a] Interestingly, for all studied anodes, the formation of IrO_3 can be determined and even correlated with electrode potential. Thus, as metallic Ir and reactively sputtered oxide have close values of potential at all current densities, the amount of IrO_3 formed is similar (Figure 2 b,c). In contrast to dissolution, the evolution of IrO_3 on thermal oxide is more intense than that observed on metallic Ir and reactively sputtered oxide. This discrepancy indicates that along with dissolution through formation of volatile Ir species another degradation route takes place that depends on a different intermediate state.

Scheme 1 presents a simplified and summarized picture of possible routes for the dissolution of iridium and its oxides during OER. The transformation of metallic Ir into IrO_2 including direct dissolution is shown in a very simplistic way assuming that at high anodic potentials the surface of the electrode should be covered with oxide. Entering the OER reaction cycle, it is well established that regardless of the electrode material the first step in acidic media is water discharge and adsorption of OH radicals on the electrode surface.[20] On Ir oxide this step is followed by the release of one electron and formation of Ir^V [Eqs. (S3) and (S4)].[13a] This type of intermediate is supposed to be involved in the OER mechanism regardless of the nature of the Ir electrode. In line with this assumption, the presence of surface Ir^V species during the OER was reported numerous times in literature.[13a,21]

The further route of both reaction paths depends on the value of the electrode potential. When the electrode potential is relatively low, decomposition of Ir^VO_2OH with release of O_2 and formation of surface $HIr^{III}O_2$ intermediates should occur [Eqs. (S5) and (S6)]. The existence of Ir^{III} and $HIr^{III}O_2$ was experimentally proven for electrochemically formed Ir oxide at relatively low overpotentials.[12,22] In further steps this metastable Ir^{III} species can either dissolve or transform into IrO_2 [Eq. (S7)]. This pathway (outlined in Scheme 1 with green arrows) is preferable for active Ir catalysts, for example, reactively sputtered IrO_2 or electrochemically formed Ir oxides. The significant dissolution of Ir for such materials suggests relatively fast kinetics of dissolution for this intermediate in comparison to oxidation. However, when the potential is high enough, further oxidation of Ir^V to Ir^{VI} is preferable [Eq. (S8)]. This second pathway (marked with red arrows in Scheme 1) thus dominates for thermal oxide at comparable current densities. For metallic Ir this reaction/dissolution route only becomes more pronounced when the potential exceeds 1.6 V_{RHE}, which is indirectly confirmed by the change of the slope of the green curve in Figure 2 a. Considering the high reactivity of IrO_3, it can either decompose to IrO_2 and O_2 [Eq. (S9)] or interact with water forming soluble IrO_4^{2-} [Eq. (S10)]. The dissolution and oxygen formation are competitive reactions, that is, the formation of an oxygen molecule does not necessary lead to dissolution of Ir. The relatively high amount of IrO_3 formed on thermal oxide together with its low dissolution rate (Figure 2) may indicate that the hydrolysis of IrO_3 has slower kinetics than its decomposition, which explains the superior stability of thermal iridium oxide. In general, the IrO_3 contribution to the overall Ir dissolution depends on the electrode potential and increases for materials with low activity towards OER. In line with our observations the Ir^V–Ir^{VI} oxidation state switch during the OER has been recently reported for Ir^V-based perovskite.[23] With the aid of XAS and TEM drastic surface reconstruction and formation of IrO_2 was also observed in this work. This agreement with the literature data suggests that the mechanisms proposed in Scheme 1 may have universal character and can be applicable to various Ir-based oxides under certain conditions. However, further research efforts are needed to prove this statement.

In conclusion, depending on the potential and surface composition of the anode, at least three different dissolution mechanisms are possible, including direct dissolution of Ir metal, the pathway through Ir^V–Ir^{III} transition, and formation of IrO_3 at high potentials. The latter two mechanisms that follow the initial surface oxidation (significant only in case of metallic Ir) are closely related to the OER reaction mechanism and share common intermediates. The electrode material determines the potential at a certain current density and thus influences the ratio between the rates of different steps as well as the stability. The dissolution route through Ir^V–Ir^{III} transformation dominates for metallic Ir and reactively sputtered oxide over other possible mechanisms. In absolute terms this pathway results in higher total dissolution. The dissolution route through Ir^V–Ir^{VI} becomes important at more positive potentials and thus in the observed cases particularly for the slightly less active thermal IrO_2. Considering the above observations, different strategies need to be developed to stabilize the respective intermediates of the reaction, in

order to increase the selectivity towards the desired product. In this context we believe that the presented fundamental results can help guide the development of more stable oxygen evolution electrocatalysts.

Acknowledgements

O.K. acknowledges the Alexander von Humboldt Foundation. We acknowledge the MAXNET Energy research initiative of the Max Planck Society for financial support. S.C. and K.J.J.M. acknowledge funding by the German Federal Ministry of Education and Research (BMBF) within the Kopernikus Project P2X.

Conflict of interest

The authors declare no conflict of interest.

Keywords: electrochemical mass spectrometry · iridium dissolution · oxygen evolution reaction · reaction mechanisms · water electrolysis

How to cite: *Angew. Chem. Int. Ed.* **2018**, *57*, 2488–2491
Angew. Chem. **2018**, *130*, 2514–2517

[1] V. R. Stamenkovic, D. Strmcnik, P. P. Lopes, N. M. Markovic, *Nat. Mater.* **2017**, *16*, 57–69.
[2] A. Grimaud, O. Diaz-Morales, B. Han, W. T. Hong, Y.-L. Lee, L. Giordano, K. A. Stoerzinger, M. T. M. Koper, Y. Shao-Horn, *Nat. Chem.* **2017**, *9*, 457–465.
[3] T. Binninger, R. Mohamed, K. Waltar, E. Fabbri, P. Levecque, R. Kotz, T. J. Schmidt, *Sci. Rep.* **2015**, *5*, 12167.
[4] Z. W. Seh, J. Kibsgaard, C. F. Dickens, I. Chorkendorff, J. K. Nørskov, T. F. Jaramillo, *Science* **2017**, *355*, eaad4998.
[5] a) G. Beni, L. M. Schiavone, J. L. Shay, W. C. Dautremont-Smith, B. S. Schneider, *Nature* **1979**, *282*, 281–283; b) O. Diaz-Morales, S. Raaijman, R. Kortlever, P. J. Kooyman, T. Wezendonk, J. Gascon, W. T. Fu, M. T. M. Koper, *Nat. Commun.* **2016**, *7*, 12363; c) L. C. Seitz, C. F. Dickens, K. Nishio, Y. Hikita, J. Montoya, A. Doyle, C. Kirk, A. Vojvodic, H. Y. Hwang, J. K. Nørskov, T. F. Jaramillo, *Science* **2016**, *353*, 1011–1014.
[6] a) S. Cherevko, S. Geiger, O. Kasian, N. Kulyk, J.-P. Grote, A. Savan, B. R. Shrestha, S. Merzlikin, B. Breitbach, A. Ludwig, K. J. J. Mayrhofer, *Catal. Today* **2016**, *262*, 170–180; b) O. Kasian, S. Geiger, P. Stock, G. Polymeros, B. Breitbach, A. Savan, A. Ludwig, S. Cherevko, K. J. J. Mayrhofer, *J. Electrochem. Soc.* **2016**, *163*, F3099–F3104; c) N. Danilovic, R. Subbaraman, K.-C. Chang, S. H. Chang, Y. J. Kang, J. Snyder, A. P. Paulikas, D. Strmcnik, Y.-T. Kim, D. Myers, V. R. Stamenkovic, N. M. Markovic, *J. Phys. Chem. Lett.* **2014**, *5*, 2474–2478.
[7] T. Reier, H. N. Nong, D. Teschner, R. Schlögl, P. Strasser, *Adv. Energy Mater.* **2017**, *7*, 1601275.
[8] A. Damjanovic, A. Dey, J. O. M. Bockris, *J. Electrochem. Soc.* **1966**, *113*, 739–746.
[9] S. Cherevko, S. Geiger, O. Kasian, A. Mingers, K. J. J. Mayrhofer, *J. Electroanal. Chem.* **2016**, *773*, 69–78.
[10] C. Spöri, J. T. H. Kwan, A. Bonakdarpour, D. P. Wilkinson, P. Strasser, *Angew. Chem. Int. Ed.* **2017**, *56*, 5994–6021; *Angew. Chem.* **2017**, *129*, 6088–6117.
[11] V. Pfeifer, T. E. Jones, J. J. Velasco Velez, C. Massue, M. T. Greiner, R. Arrigo, D. Teschner, F. Girgsdies, M. Scherzer, J. Allan, M. Hashagen, G. Weinberg, S. Piccinin, M. Havecker, A. Knop-Gericke, R. Schlogl, *Phys. Chem. Chem. Phys.* **2016**, *18*, 2292–2296.
[12] A. Minguzzi, O. Lugaresi, E. Achilli, C. Locatelli, A. Vertova, P. Ghigna, S. Rondinini, *Chem. Sci.* **2014**, *5*, 3591–3597.
[13] a) H. G. Sanchez Casalongue, M. L. Ng, S. Kaya, D. Friebel, H. Ogasawara, A. Nilsson, *Angew. Chem. Int. Ed.* **2014**, *53*, 7169–7172; *Angew. Chem.* **2014**, *126*, 7297–7300; b) V. Pfeifer, T. E. Jones, J. J. Velasco Vélez, C. Massué, R. Arrigo, D. Teschner, F. Girgsdies, M. Scherzer, M. T. Greiner, J. Allan, M. Hashagen, G. Weinberg, S. Piccinin, M. Hävecker, A. Knop-Gericke, R. Schlögl, *Surf. Interface Anal.* **2016**, *48*, 261–273.
[14] S. Cherevko, S. Geiger, O. Kasian, A. Mingers, K. J. J. Mayrhofer, *J. Electroanal. Chem.* **2016**, *774*, 102–110.
[15] R. Kötz, H. Neff, S. Stucki, *J. Electrochem. Soc.* **1984**, *131*, 72–77.
[16] M. Wohlfahrt-Mehrens, J. Heitbaum, *J. Electroanal. Chem.* **1987**, *237*, 251–260.
[17] O. W. J. Willsau, J. Heitbaum, *J. Electroanal. Chem. Interfacial Electrochem.* **1985**, *195*, 299–306.
[18] K. Macounova, M. Makarova, P. Krtil, *Electrochem. Commun.* **2009**, *11*, 1865–1868.
[19] S. Fierro, T. Nagel, H. Baltruschat, C. Comninellis, *Electrochem. Commun.* **2007**, *9*, 1969–1974.
[20] J. O. Bockris, *J. Chem. Phys.* **1956**, *24*, 817–827.
[21] A. Minguzzi, C. Locatelli, O. Lugaresi, E. Achilli, G. Cappelletti, M. Scavini, M. Coduri, P. Masala, B. Sacchi, A. Vertova, P. Ghigna, S. Rondinini, *ACS Catal.* **2015**, *5*, 5104–5115.
[22] J. D. E. McIntyre, S. Basu, W. F. Peck, W. L. Brown, W. M. Augustyniak, *Phys. Rev. B* **1982**, *25*, 7242–7254.
[23] A. Grimaud, A. Demortière, M. Saubanère, W. Dachraoui, M. Duchamp, M.-L. Doublet, J.-M. Tarascon, *Nat. Energy* **2016**, *2*, 16189.

Manuscript received: September 18, 2017
Accepted manuscript online: December 8, 2017
Version of record online: February 5, 2018

